Aging and Phase Separation of Elastomers Investigated by NMR Imaging

P. Blümler and B. Blümich*

Max-Planck-Institut für Polymerforschung, D-6500 Mainz, Germany

Received June 4, 1990; Revised Manuscript Received November 2, 1990

ABSTRACT: Proton spin–echo imaging has been applied to investigations of aging and phase separation in elastomeric materials. Vulcanized natural rubber filled with carbon black was aged in air at elevated temperature. A diffusion-controlled hardening of the surface layer was observed. Its radial growth was studied, and the local kinetics of the aging reaction were followed by spin–echo and T_2 images. By the same techniques, inhomogeneities in the natural rubber were detected and characterized. Phase separation of a model mixture of a stearic acid and paraffin was monitored in three dimensions by multislice imaging, and the phase separation of a polyisoprene and polystyrene blend was observed by difference images with a spatial resolution of $30 \times 30 \times 300$ μm^3.

Introduction

NMR imaging is an established method in medical diagnostics.[1,2] Presently, various efforts are being reported to adapt this technique to materials science.[3–15] The advantages of NMR imaging are, above all, the nondestructiveness, the abundance of detectable molecular parameters, and the lack of ionizing radiation. The NMR signal of mobile molecules, for instance in liquids and most biological samples, depends not only on the local spin density but also on the spin–lattice relaxation time T_1, the spin–spin relaxation time T_2, and the chemical shift. However, application of liquid-state imaging techniques to solids often is problematic.

As the NMR frequency is proportional to the magnetic field, spatial resolution is achieved by measurement in a field gradient. The resolution depends on the line width of the investigated substance. In rigid solids the molecular mobility is restricted, and broad lines, typically 5–50 kHz for protons, are observed mainly as a result of the homonuclear dipolar coupling and to a lesser degree the chemical shift and anisotropic magnetic shielding. In liquids and many biological samples, on the other hand, the molecular mobility is high, and the interactions are averaged to their isotropic values. As a result, narrow line widths of only a few hertz are observed. Spatial resolution of about $10 \times 10 \times 100$ μm^3 can be achieved.[3] For this reason, many investigations of NMR imaging to material science are restricted to samples with high molecular mobility, for instance the distribution of liquids in porous rocks,[16–18] ceramics,[5,19–25] wood[26,27] and other plant materials,[28–30] and synthetic polymers.[14,15,31–36]

To image solid materials, different approaches can be taken. For example, the gradient effect can be increased by creating stronger gradient fields[37,38] or by exploiting multiquantum coherences.[39–41] Line narrowing can be achieved by magic angle spinning (MAS)[9,42–45] or multipulse techniques[8,46,47] also in combination with MAS or by the use of echoes.[48] Finally, conventional liquid-state NMR imaging methods[12,49–52] can be used for investigating solids with narrow lines. Such materials include elastomers with a glass transition temperature well below the temperature of investigation. Their natural line width ranges from about 500 to 2000 Hz. Chang and Komoroski[12] have studied the use of NMR imaging for the investigation of elastomeric materials. They compared gradient–echo and spin–echo techniques in terms of contrast and resolution and discussed the detection of defects such as voids, gaps, or small foreign particles in elastomers, as well as chemical shift and susceptibility artifacts.

In this work spin–echo imaging is applied to investigate the physical aging of cross-linked caoutchouc (vulcanized natural rubber). Aging studies often are based on statistical grounds. Large numbers of samples are required and analyzed at different times of the aging process.[53–58] In most cases the analysis destroys the sample. The nondestructive character of NMR imaging provides a profitable and elegant way to monitor various changes in the material properties of a single sample. In the following the segmental mobility in the aged polymer network and the kinetics of the degradation reaction are investigated as a function of the aging time for the same sample.

Furthermore, the phase separation of a model system and that of a polymer blend with one elastomeric component are analyzed by conventional spin–echo imaging. Phase separation of polymer blends is a process of considerable technical interest.[59–61] The analysis of separation processes with NMR imaging seems to be restricted to features above the spatial resolution limit of presently about $10 \times 10 \times 100$ μm^3. It is shown that difference images are sensitive to morphological changes below the spatial resolution limit. This technique is complementary to the detection of phase separation in blends by MAS imaging.[9] It illustrates the use of conventional NMR imaging for the investigation of slow time-dependent processes on the time scale of hours.

All NMR experiments were performed at 300.1 MHz with a Bruker MSL spectrometer equipped with a microimaging probe.

Experimental Section

Aging of Vulcanized Natural Rubber. (a) Pulse Sequence. For the aging studies a conventional multiecho pulse sequence[2,62] was used. Repeated refocusing of the echo[63] allows for the determination of the spin–spin relaxation time T_2 by calculating the time constant of the exponential decay of the spin–echo amplitude. The sequence of radio frequency and field gradient pulses used is depicted in Figure 1 for reference and identification of parameters. Radio frequency pulse lengths and gradient switching times restricted the measurement of T_2 relaxation times to values above 1 ms. Low signal strength, however, required long measurement times of the order of about 10 h per image. The gradient strengths were as follows: *read* gradient $G_{x2} = 250$ mT/m; maximum amplitude of the *phase encoding* gradient $G_y = 250$ mT/m; and *slice selection* gradient $G_z = 150$ mT/m. In the presence of G_z the 180° selective pulse P2 (bandwidth ca. 6000 Hz) generates a slice in the z direction of about 1 mm. The spatial resolution limit (80×80 μm^2) in the

0024-9297/91/2224-2183$02.50/0

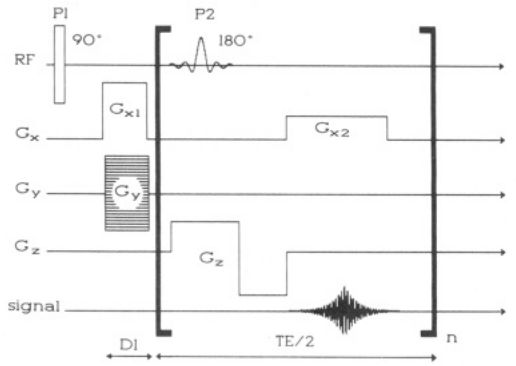

Figure 1. Timing diagram of the basic spin–echo sequence used for 2D FT NMR imaging.

x,y plane is determined by G_{x2} and G_y and the natural line width of the sample. The data for the images were acquired on a 128 × 128 point mesh resulting in a pixel size of about 75 × 75 μm^2.

(b) Sample Preparation. A cylindrical sample (5-mm diameter) of natural rubber filled with carbon black was provided from the Bayer Co., Leverkusen, FRG. The sample was removed after each measurement and aged for a predetermined period of time in an air-filled drybox at 130 °C. After each aging period, the sample was packed into a glass tube along with an unaged reference sample and a contrast agent. Measurements were made at room temperature.

The contrast agent was required to outline the sample contours, since in the images the aged material as well as empty space appears black due to very low or no signal intensity for these regions. The agent was an emulsion of D_2O, liquid paraffin, and potassium palmitate. The composition of the agent was optimized to match the chemical shift of the rubber so as to minimize artifacts in the images. Diffusion of the aqueous contrast emulsion into the rubber sample was not observed in a control NMR imaging experiment over a time as long as 2 days.

Segregation of a Stearic Acid and Paraffin Mixture. (a) Pulse Sequence. The same basic pulse sequence (Figure 1) was used, but only one echo ($n = 1$) was observed and the frequency of the selective pulse P2 was varied so as to select different slices in the sample (multislice technique). In this way the three-dimensional structure of the sample was investigated in terms of parallel cross sections. With a bandwidth of about 1000 Hz for the selective pulse and G_z = 180 mT/m, the thickness of a cross section was 130 μm, given a natural line width on the order of 100 Hz for the stearic acid and paraffin mixture at room temperature. These slices were spaced 250 μm apart, and with $G_{x2} = G_y$ = 200 mT/m, the "natural" resolution in each dimension of the slice plane was calculated to be about 12 μm. But the data matrix sizes for this experiment were of 256 × 256 pixels, so the pixel size is about 45 × 45 μm^2, determining the real resolution limit for this experiment. Measurement of one slice required 1 h.

(b) Sample Preparation. Equal volumes of stearic acid (T_m = 71 °C) and liquid paraffin (Merck $d_{20°C}$ = 0.88) were melted together. The warm melt was poured into a glass tube of 7-mm diameter and slowly cooled to room temperature. The resulting sample was opalescent and appeared to be homogeneous.

Phase Separation of a Polyisoprene and Polystyrene Blend. (a) Pulse Sequence. This process was studied with the basic spin–echo sequence (Figure 1). Since the expected structures are very small, gradient strengths corresponding to $G_x = G_y$ = 500 mT/m and G_z = 300 mT/m have been applied. The maximum achievable resolution was calculated to be 30 × 30 × 300 μm^3 given the natural line width of polyisoprene of ca. 600 Hz and a width of 1 ms of the selective pulse P2. The measurement time was 10 h for each image.

(b) Sample Preparation. Equal amounts of polyisoprene (SKI3S) and polystyrene (M_w = 346 000; U = 1.3) were dissolved in chloroform. The solutions were mixed, precipitated into methanol, and dried under vacuum at room temperature. The resulting blend was very elastic and difficult to mold. The sample chosen for this experiment had a diameter of 2 mm and was quite inhomogeneous. It was arrested in a small glass tube with a PTFE plug, prior to insertion of the tube into the probe.

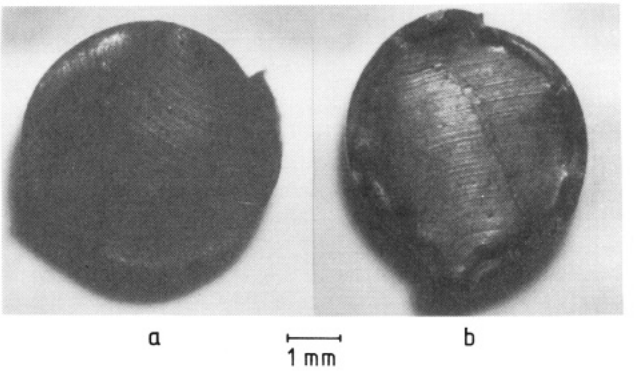

Figure 2. Photographs of the natural rubber samples filled with carbon black. (a) Unaged. (b) Aged for 48 h at 130 °C in air. The hard layer at the surface could be contrasted by sideward lighting. The small grooves resulted from cutting.

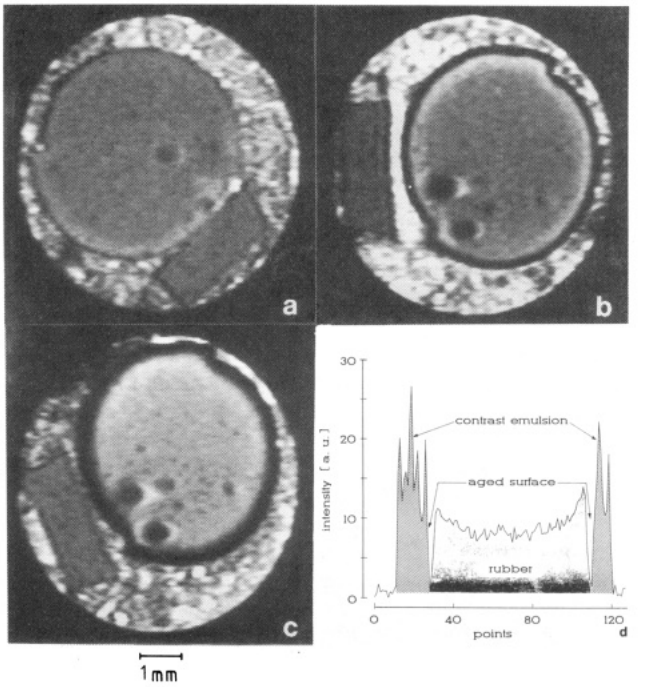

Figure 3. Axial spin–echo images of vulcanized natural rubber (circular object) for different aging times. The dark ring near the surface is a hard layer formed by the aging process at T = 130 °C. The square object is an unaged reference sample with a rectangular cross section of 1 × 3 mm^2. Both are embedded in a bright viscous contrast agent which appears inhomogeneous because it is foamy and includes small air bubbles. The aging times are 2, 8, and 34 h for (a), (b), and (c), respectively. (d) Horizontal profile of the image in Figure 3b (row 76) documenting the steepness in the contrast between aged and unaged rubber.

Results and Discussion

Aging of Natural Rubber. It was not possible to visually ascertain any conspicuous change on the surface of the aged natural rubber up to aging times of about 8 h. At longer times, the sample became noticeably harder, and a hardened surface layer can be seen by visual inspection of the cross section after cutting (Figure 2). The shape of the sample was not affected by the aging process. Figure 3 shows the images generated from the first echo for aging times of 2, 8, and 34 h, respectively. They were chosen from a series of 10 measurements. Since the sample was removed for aging between the measurements, the physical positioning in the glass tube was not reproducible exactly. Inspecting these figures, it is noted that small air bubbles in the viscous contrast agent cause the background to appear different in each image.

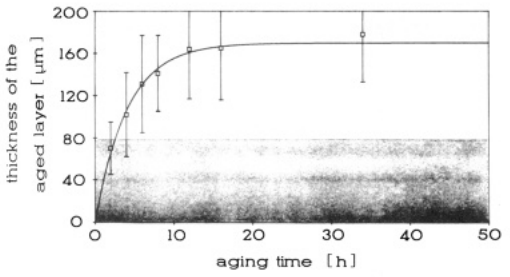

Figure 4. Dependence of the thickness of the aged layer on the aging time. The shaded region marks the spatial resolution limit.

The large, circular object in the middle of each image is the rubber sample. Two small bulges at the upper and lower ends of the sample are recognizable. These resulted from the particular molding process. Furthermore, inhomogeneities of varying size are perceptible as dark spots with bright shadows inside the aged sample. The shadows are artifacts which arise from the difference in susceptibility[64] of the inhomogeneities in comparison to the surrounding rubber. The square object is the unaged reference sample.

The rubber images show dark rings of different thickness near the surface. These rings are not susceptibility artifacts, since they do not appear as shadows in one space dimension like the contours of the inhomogeneities. In Figure 3a, this ring is almost imperceptible. It is more pronounced in Figure 3b and has reached considerable thickness in Figure 3c. This ring is an aged surface layer which is not only growing but also becoming harder with increasing aging time. The sharp contrast between aged outer and unaged inner material is quite remarkable and provides an accurate criterium for measuring its width (Figure 3d).

By careful inspection a brighter ring is detected at the interface of the dark ring and the unaged material in the interior of the sample. It may be explained either by stabilizers like stearin and paraffin, which diffuse to the reaction front, or by increased mobility of rubber segments due to chain rupture, which precedes the cross-linking stage in the aging process. A more detailed investigation is in progress.

(a) Growth of the Surface Layer. To follow the growth of the layer, a cross-sectional image was measured. The thickness of the aged mantle was determined by eyeball-fitting of two circles with variable centers and diameters to the inner and outer outlines of the aged layer. This was done with software written in PV-WAVE on a Vax workstation. From the resultant area in between the two circles the average diameter was calculated. Figure 4 shows the dependence of the thickness on the aging time. The onset of the aging process can be observed by NMR after the sample has been aged as little as 2 h. This is considerably earlier than is observable by visual means (ca. 8 h, see above), but the diameter then is near the spatial resolution limit. The layer growth is fast initially and slow later. Such behavior is reminiscent of the corrosion for some metals, i.e., the formation of an oxidative, impervious layer, which prevents the diffusion of oxygen into the material. Evans[65] and Wiederholdt[66] have shown that the thickness r of such a radial protective film exhibits an asymptotic behavior.

$$r(t) = r(t \rightarrow \infty)(1 - e^{-t/T_r}) \quad (1)$$

This equation describes the initial rise of the measured diameters very well (Figure 4). A fit to the experimental data yields a saturation diameter $r(t \rightarrow \infty)$ of 170 μm and a time constant T_r of 4 h. The first value of the layer thickness in Figure 4 is lower than the spatial resolution limit. Such values are meaningful, since they are averaged values obtained from the cross-sectional area of the aged material. Also it is known that structures smaller than the pixel resolution can lead to changes in the image contrast.[12]

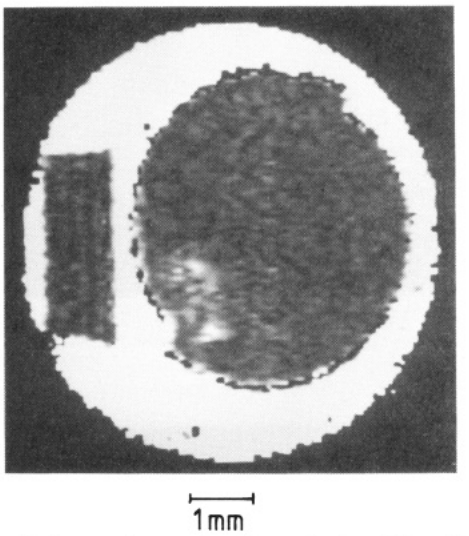

Figure 5. T_2 image of natural rubber, calculated from four spin–echoes (Figure 3b displays the first of the four) produced by a multiecho sequence. The aging time is 8 h.

(b) T_2 Characteristics. In addition to the spin density T_2 already enters into the contrast of the images in Figure 3. Thus, a qualitive discussion is possible with these T_2-weighted images. The fact that the aged surface layer appears much darker while a significant decrease in the proton density by aging can be excluded suggests a decrease of the T_2 relaxation time. A more detailed understanding is gained by calculating pure "T_2 images" from the decay of the echo amplitudes measured by multiecho imaging. In T_2 images every shade of gray corresponds to a different T_2 value. Figure 5 shows an example for one selected aging time. The image exhibits much more contrast than the spin–echo images in Figure 3, but it is more noisy because the signal-to-noise ratio decreases with decreasing T_2 and increasing echo times. The small air bubbles in the contrast agent have vanished from the image. Since they are smaller than the pixel resolution, they only affect the spin density[12] and not the relaxation time in the pixel.

The inhomogeneities in the rubber, which can be recognized as dark spots in Figure 3, now appear brighter in Figure 5 than the rubber in the center of the sample. This corresponds to a longer T_2 relaxation time (ca. 11 ms). However, the inhomogeneities must have a lower proton density than the normal rubber; otherwise, their low intensity in the spin–echo images (Figure 3) cannot be explained. Furthermore, with increasing aging time an increase in the T_2 of the rubber inhomogeneities is observed. This suggests that they collect mobile components during the aging process. The inhomogeneities could be discerned upon magnification but proved to be too small for chemical analysis. It is likely that they are carbon black particles in the rubber matrix, which absorb some liquid components of the rubber (paraffin, stearin, and low molecular weight aging products[55]).

(c) Reaction Kinetics. The aging reaction can approximately be described by

$$\mathrm{U} + \mathrm{O}_2 \xrightarrow[k]{\Delta} \mathrm{A} \quad (2)$$

The soft, unaged rubber U reacts with oxygen at elevated

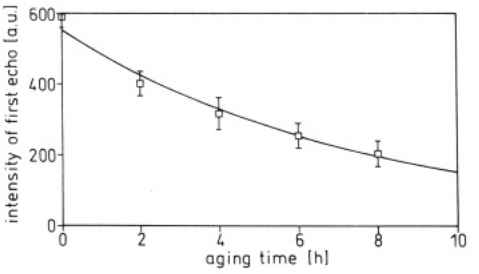

Figure 6. Plot of the amplitude of the first echo for the aged surface layer vs the aging time. The curve was calculated according to eq 4 for the simplified aging reaction 2.

temperature to the harder, aged material A. In this simple model segments of the network can assume only two possible states, i.e., soft and hard. These two states show two different segmental mobilities. Since the T_2 relaxation time corresponds to molecular mobility, these states are characterized by two different relaxation times. For the unaged rubber T_{2U} = 5.8 ms and for the aged rubber T_{2A} = 0.3 ms have been determined. These relaxation times differ by more than 1 order of magnitude, so that the amplitude of the first echo (acquired 4.4 ms after the 90° pulse) to a good degree of approximation already results from the unaged segments with relaxation time T_{2U} only.

If reaction 2 can be described by first-order kinetics with the reaction rate constant k, the concentration dependence of the unaged rubber [U] on the aging time t_a can be expressed by[67]

$$[U](t_a) = [U](t_a=0)e^{-kt_a} \tag{3}$$

Then the amplitude $M(t_e,t_a)$ of the echo acquired at t_e becomes a function of the aging time:

$$M(t_e,t_a) = M_0 e^{-kt_a} e^{-t_e/T_{2U}} \tag{4}$$

In this equation all parameters are known except M_0 and k, which can be determined by a logarithmic plot of the echo amplitude vs the aging time, resulting in a value of k^{-1} = 8 h ± 30% for the inverse reaction rate constant. Figure 6 shows the first five echo amplitudes and a fit of eq 4 to the experimental data. An error of about 30% for a reaction rate is acceptable. Comparison of the inverse rate, i.e., the time constant of the aging reaction, with the value of 4 h found for T_r shows that the hardening proceeds half as fast as the growth of the aged surface layer.

Segregation of a Stearic Acid and Paraffin Mixture. The solution of stearic acid in paraffin was observed to be homogeneous at temperatures above 37 °C (Figure 7a). At lower temperatures the stearic acid separates out, appearing as the dark structure in the middle of the images (Figure 7b–e). The darker color indicates faster T_2 relaxation as compared to that of the surrounding stearin solution. The multiple slices convey the form of the separated stearin in three dimensions. To verify that the dark structure in the center was not an air bubble or a quenching channel, the sample was first cut and then heated. At 37 °C the core dissolved.

This imaging experiment illustrates the possible use of the method for investigations of separation and crystallization phenomena. When small structures are studied, it is important to be aware of the fact that the in-plane resolution often is far better than the out-of-plane resolution. This is because the selective pulse must be shorter than the signal decay. Since the length of the selective pulse is inversely proportional to the thickness of the selected slice, for short T_2, a compromise between signal-to-noise ratio and slice thickness must be made, and structures that are homogeneous in at least one dimension

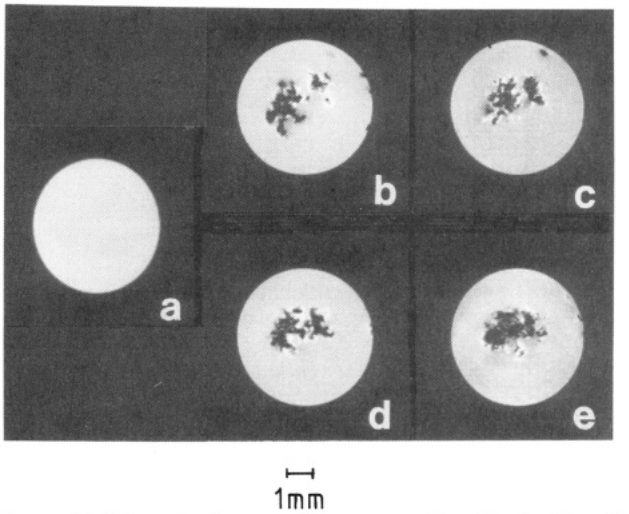

Figure 7. Spin–echo images of the segregation of a stearic acid and paraffin model mixture measured by the multislice technique. (a) Homogeneous melt at 37 °C. (b–e) Segregation due to the precipitation of stearic acid in the saturated mixture at 28 °C in different slices. Slice thickness, 130 μm; slice separation, 250 μm; spatial in-plane resolution, 45 × 45 μm² in 256 × 256 pixels.

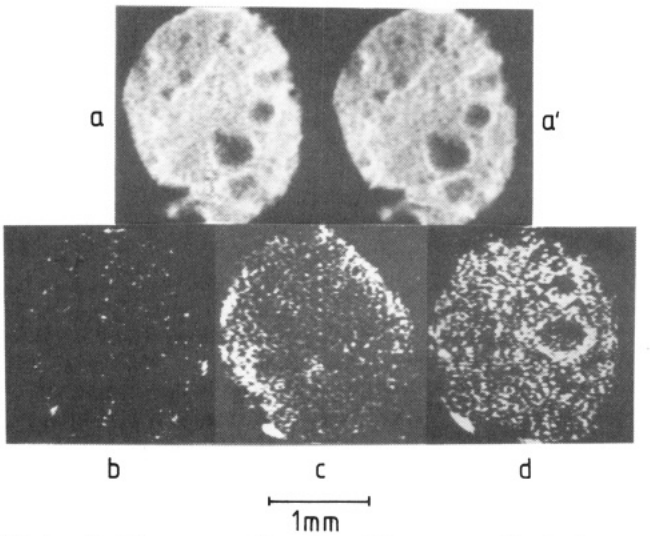

Figure 8. Phase separation of a polyisoprene and polystyrene blend at 25 °C. (a, a') Two separately measured spin–echo images of the same sample. (b) Difference image of (a) displaying measurement noise for reference. (c) Difference image after the sample was heated to 80 °C for 10 h. (d) Difference image after the sample was heated to 100 °C for 10 h.

can readily be studied. This situation is applicable to the rubber aging studies above.

Phase Separation of a Polyisoprene and Polystyrene Blend. The phase separation of polymer blends is very difficult to observe with NMR imaging techniques, because the process is inhomogeneous in all three dimensions and the structures are small, but the selected slices have to be thick for good signal levels. For reasons of resolution MAS imaging has been applied for the detection of phase separation of polybutadiene and polystyrene blends. But even for comparatively large structures, the image intensity is determined by the sum of signals from many small structures as the result of low out-of-plane resolution.[9]

However, phase separation can even be observed in favorable cases with conventional spin–echo techniques if difference images are computed. This is demonstrated in Figure 8 by spin–echo images of a polyisoprene and polystyrene blend. The voids that can be recognized in

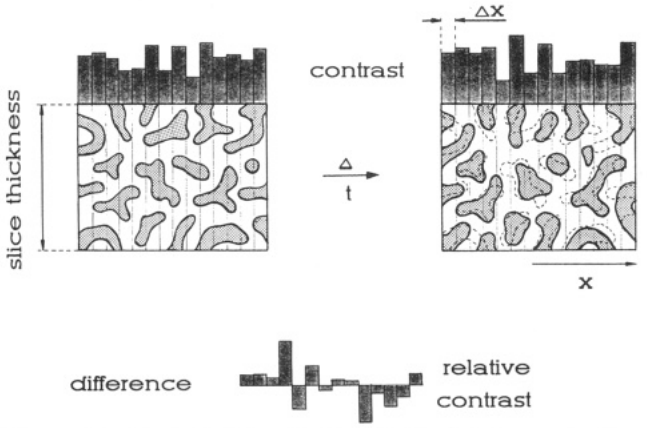

Figure 9. (Top) Profiles of a hypothetical, interpenetrating network of separated phases and the schematically detected image profile for two different arrangements due to two different states in the separation process. (Bottom) Difference of the upper two image profiles reveals the change resulting from motion of the phase boundaries.

the two images in parts a and a′ Figure 8 are due to air bubbles generated by the pressing and molding processes. Both images were obtained from two identical measurements of the sample at ambient temperature. Their difference (Figure 8b) is a measure of reproducibility.

The noise level indicates that the reproducibility is good. Parts c and d of Figure 8 are difference images measured at ambient temperature, with the sample having been heated between measurements to 80 (Figure 8c) and 100 °C (Figure 8d) for ca. 10 h in the probe. Since the difference images are measured at different occasions, the sample was removed from the magnet in the mean time, and the difference images of Figure 8b–d show different parts of the sample. The contrast in these images increases from Figure 8b to Figure 8d, indicating a motion of boundaries between domains of different signal intensities as a changing sum of signals across the slice thickness. This is illustrated schematically in Figure 9. Under the experimental conditions used here, the in-plane resolution (30 μm) was 10 times higher than the out-of-plane resolution (300 μm) determined by the signal fluctuation of the sum over polyisoprene (dark) and polystyrene (bright) domains. As the domain sizes increase, these fluctuations became larger as well. The difference image then displays the difference in signal fluctuation as a measure of the time-dependent change in the sample. These results are in agreement with results from light microscopy.[61] However, it cannot completely be excluded that the observed change of boundaries is not affected by air bubbles in the blend expanding during the heating process.

Summary and Conclusion

Conventional NMR imaging techniques have been applied to investigate homogeneity, reaction rates, and phase separation phenomena in solid materials with mobile components. While the spatial resolution cannot compete with other microscopic methods, these experiments demonstrate potential use of NMR imaging for nondestructive material analysis.

The characterization of inhomogeneities by NMR imaging is a valuable application of nondestructive material testing, but the aging and phase separation studies showed that the identification of heterogeneous dynamic processes by specific NMR parameters may be more important. In principle, it is possible to observe the aging process by light microscopy, but an optical contrast must be generated and the growth of aged surface layers often cannot be observed on the same sample. The analysis of the aging process demonstrates that determination of molecular dynamics is possible by NMR imaging. In general, a kinetic map of the sample can be generated.

Phase structures down to 30 μm were detected in separation processes under favorable conditions. These conditions are homogeneity in one direction and long T_2 times. Even if the desired homogeneity does not exist, it was demonstrated that small structures can be resolved by measuring their morphological change and displaying the result in terms of difference images. The disadvantages of this technique include measurement times of several hours and the use of expensive instrumentation.

This work represents an exploratory study of the potential use of NMR imaging to materials-related questions. More work needs be done to take advantage of the vast possibilities offered by NMR imaging in polymer science. Applications are expected in such diverse fields as aging of elastomers under static and dynamic stress and different environmental conditions, distributions of chemical reactions, and investigations of stress and temperature a functions of time, shape, and boundary conditions, but for solids with highly restricted molecular mobility different approaches to solid-state imaging must be developed.

Acknowledgment. We thank Dr. A. Zembrod and Dr. U. Eisele, Bayer AG, Leverkusen, for providing different samples of natural rubbers. We acknowledge the continuous interest and support of this work by Prof. Dr. H. W. Spiess, and we thank him and Dr. G. G. Maresch for helpful discussions of the aging results.

References and Notes

(1) Mansfield, P.; Morris, P. G. *Advances in Magnetic Resonace*; Academic Press: New York, 1982; Suppl. 2.
(2) Wehrli, F. W.; Shaw, D.; Kneeland, J. B. *Biomedical Magnetic Resonance Imaging*; VCH: Weinheim, 1988.
(3) Kuhn, W. *Angew. Chem.* **1990**, *102*, 1–20.
(4) Jelinski, L. W.; Cockman, M. D. *Polym. Prepr.* **1990**, *31*, 100.
(5) Ackerman, J. L.; Garrido, L.; Moore, J. E.; Ellingson, W. A. *Polym. Prepr.* **1990**, *31*, 145.
(6) Callaghan, P. T. *Bull. Magn. Reson.* **1989**, *11*, 216.
(7) Listerud, J. M.; Sinton, S. W.; Drobny, G. P. *Anal. Chem.* **1989**, *23A*, 61.
(8) Miller, J. B.; Garroway, A. N. *Rev. Prog. Quant. Nondestr. Eval.* **1988**, *7A*, 287.
(9) Cory, D. G.; de Boer, J. C.; Veeman, W. S. *Macromolecules* **1989**, *22*, 1618.
(10) Weisenberger, L. A.; Koenig, J. L. *Appl. Spectrosc.* **1989**, *43*, 1117.
(11) Hoh, K. P.; Perry, B.; Rotter, G.; Ishida, H.; Koenig, J. L. *J. Adhes.* **1989**, *27*, 245.
(12) Chang, C.; Komoroski, R. A. *Macromolecules* **1989**, *22*, 600.
(13) Blümich, B. *Angew. Chem.* **1989**, *100*, 1460.
(14) Jackson, P.; Clayden, N. J.; Walton, N. J.; Carpenter, T. A.; Hall, L. D.; Jezzard, P.; Wiggins, C. Poster C6, 10th European Experimental NMR Conference, Veldhoven, The Netherlands, 1990.
(15) Jackson, P.; Clayden, N. J.; Carpenter, T. A.; Hall, L. D.; Jezzard, P. Poster C7, 10th European Experimental NMR Conference, Veldhoven, The Netherlands, 1990.
(16) Hall, L. D.; Rajanayagam, V.; Halls, C. *J. Magn. Reson.* **1986**, *68*, 185.
(17) Gaigalas, A. K.; Van Orden, A. C.; Robertson, B.; Marceci, T. H.; Lewis, L. A. *Nucl. Technol.* **1989**, *84*, 113.
(18) Guillot, G.; Trokiner, A.; Darasse, L.; Saint-Jalmes, H. *J. Phys. D: Appl. Phys.* **1989**, *22*, 1646.
(19) Ackerman, J. L.; Ellingson, W. A.; Koucher, J. A.; Rosen, B. R. In *Nondestructive Characterization of Materials II*; Bussiere, J. F., Monchalin, J. P., Rund, C. O., Green, R. E., Jr., Eds.; Plenum Press: New York, 1987.
(20) Ellingson, W. A.; Ackerman, J. L.; Garrido, L.; Weyand, J. D.; DiMilia, R. A. *Ceram. Eng. Sci. Proc.* **1987**, *8*, 503.

(21) Garrido, L.; Ackerman, J. L.; Ellingson, W. A.; Weyand, J. D. *Ceram. Eng. Sci. Proc.* **1988**, *9*, 1465.
(22) Ackerman, J. L.; Garrido, L.; Ellingson, W. A.; Weyand, J. D. In *Nondestructive High Performance Ceramics*; American Chemical Society: Washington, DC, 1988.
(23) Ellingson, W. A.; Wong, P. S.; Dieckmann, S. L.; Ackerman, J. L.; Garrido, L. *Am. Ceram. Bull.* **1989**, *68*, 1180.
(24) Garrido, L.; Ackerman, J. L.; Ellingson, W. A. *J. Magn. Reson.* **1990**, *88*, 340.
(25) Hayashi, K.; Kawashima, K.; Kose, K.; Inouye, T. *J. Phys. D: Appl. Phys.* **1988**, *21*, 1037.
(26) Hall, L. D.; Rajanayagam, V. *Wood Sci. Technol.* **1986**, *20*, 329.
(27) Chang, S. U.; Olson, J. R.; Wang, P. C. *For. Prod. J.* **1989**, *39*, 43.
(28) Johnson, G. A.; Brown, J.; Kramer, P. J. *Proc. Natl. Acad. Sci. U.S.A.* **1987**, *84*, 2752.
(29) Eccles, C. D.; Callaghan, P. T.; Jenner, C. F. *Biophys. J.* **1988**, *53*, 77.
(30) Cofer, G. P.; Brown, J. M.; Johnson, G. A. *J. Magn. Reson.* **1989**, *83*, 608.
(31) Suits, B. H.; White, D. *Solid State Commun.* **1984**, *50*, 291.
(32) Blackband, S.; Mansfield, P. *J. Phys. C: Solid State Phys.* **1986**, *19*, L49.
(33) Rothwell, W. P.; Holecek, D. R.; Kershaw, J. A. *J. Polym. Sci., Polym. Lett. Ed.* **1984**, *22*, 241.
(34) Mareci, T. H.; Donstrup, S.; Rigamonti, A. *J. Mol. Liq.* **1988**, *38*, 185.
(35) Tabak, F.; Corti, M. *J. Chem. Phys.* **1990**, *92*, 2673.
(36) Weisenberger, L. A.; Koenig, J. L. *J. Polym. Sci., Part C: Polym. Lett.* **1989**, *27*, 55.
(37) Samoilenko, A. A.; Artemov, D. Y.; Sibel'dina, L. A. *JETP Lett.* **1988**, *47*, 348.
(38) Samoilenko, A. A.; Zick, K. *Bruker Rep.* **1990**, *1*, 40.
(39) Garroway, A. N.; Baum, J.; Munowitz, M. G.; Pines, A. *J. Magn. Reson.* **1984**, *60*, 337.
(40) Emid, S. *Phys. B+C (Amsterdam)* **1985**, *128*, 79.
(41) Günther, E.; Blümich, B.; Spiess, H. W. *Mol. Phys.*, submitted for publication.
(42) Veeman, W. S.; Cory, D. G. *Adv. Magn. Reson.* **1989**, *13*, 43.
(43) Cory, D. G.; Veeman, W. S. *J. Phys. E: Sci. Instrum.* **1989**, *22*, 180.
(44) Matsui, S.; Sekihara, K.; Shiono, H.; Kohno, H. *J. Magn. Reson.* **1988**, *77*, 182.
(45) Ogura, Y.; Sekihara, K. *J. Magn. Reson.* **1989**, *83*, 177.
(46) Miller, J. B.; Cory, D. G.; Garroway, A. N. *Polym. Prepr.* **1990**, *31*, 143.
(47) Cory, D. G.; Miller, J. B.; Turner, R.; Garroway, A. N. *Mol. Phys.* **1990**, *70*, 331.
(48) Rommel, E.; Hafner, S.; Kimmich, R. *J. Magn. Reson.* **1990**, *86*, 264.
(49) Chang, C.; Komoroski, R. A. *Polym. Prepr.* **1988**, *29*, 94.
(50) Clough, R. S.; Koenig, J. L. *J. Polym. Sci., Part C: Polym. Lett.* **1989**, *27*, 451.
(51) Webb, A. G.; Jezzard, P.; Hall, L. D.; Ng, S. *Polym. Commun.* **1989**, *30*, 363.
(52) Garrido, L.; Ackerman, J. L.; Chang, C.; Mark, J. E. *Polym. Prepr.* **1990**, *31*, 147.
(53) Fisher, L. *Chemistry of Natural and Synthetic Rubbers*; Reinhold: New York, 1957; Chapter 7.
(54) Kern, W. *Chem.-Ztg., Chem. Appar.* **1967**, *91*, Heft 9, 255–262.
(55) Brydson, J. A. *Rubber Chemistry*; Applied Science: London, 1978; Chapter 9.
(56) Pinner, S. H. *Weathering and Degradation of Plastics*; Columbine: London, 1966; Chapter 1.
(57) Grosser, B.; *Diplomarbeit*; Pädagogische Hochschule: Erfurt/Mühlhausen, 1986; Kapitel 4.
(58) Breuers, W.; Luttropp, H. *Buna*; Verlag Technik: Berlin, 1954; Kapitel 2.
(59) Olagoke, O. *Encycl. Chem. Technol.* **1982**, *18*, 443.
(60) Schmidt-Rohr, K.; Clauss, J.; Blümich, B.; Spiess, H. W. *Magn. Reson. Chem.*, in press.
(61) Gergen, W. P.; Davison, S.; Lutz, R. G. In *Thermoplastic Elastomers—Research and Development*; Legge, N. R., Eds.; Hanser: München, 1986.
(62) Liu, J.; Nieminen, A. O. K.; Koenig, J. L. *J. Magn. Reson.* **1989**, *85*, 95.
(63) Carr, H. Y.; Purcell, E. M. *Phys. Rev.* **1954**, *94*, 630.
(64) Henkelman, R. M.; Bronskill, M. J. *Rev. Magn. Reson. Med.* **1987**, *2*, (1), 44.
(65) Evans, U. R. *The Corrosion and Oxidation of Metalls*; Arnold: London, 1960; Chapter 20.
(66) Wiederholdt, W. *Korrosionsprüfverfahren*; Verlag Chemie: Berlin, 1945; p 11.
(67) Frost, A. A.; Pearson, R. G. *Kinetik und Mechanismen homogener chemischer Reaktionen*; Verlag Chemie: Weinheim, 1964.

Registry No. Polystyrene, 9003-53-6; stearin, 11099-07-3.